Journal of Solid State Chemistry 182 (2009) 698–708

Contents lists available at ScienceDirect

Journal of Solid State Chemistry

journal homepage: www.elsevier.com/locate/jssc

Preparation and luminescence properties of Ce^{3+} and/or Tb^{3+} doped $LaPO_4$ nanofibers and microbelts by electrospinning

Zhiyao Hou [a,b], Lili Wang [b], Hongzhou Lian [b], Ruitao Chai [b], Cuimiao Zhang [b], Ziyong Cheng [b], Jun Lin [b,*]

[a] College of Materials Science and Chemical Engineering, Harbin Engineering University, Harbin 150001, PR China
[b] State Key Laboratory of Rare Earth Resource Utilization, Changchun Institute of Applied Chemistry, Chinese Academy of Sciences, Changchun 130022, PR China

ARTICLE INFO

Article history:
Received 16 October 2008
Received in revised form
9 December 2008
Accepted 15 December 2008
Available online 4 January 2009

Keywords:
Electrospinning
$LaPO_4$ nanofiber
$LaPO_4$ microbelt
Phosphor

ABSTRACT

Ce^{3+} and/or Tb^{3+} doped $LaPO_4$ nanofibers and microbelts have been prepared by a combination method of sol-gel process and electrospinning. X-ray diffraction (XRD), scanning electron microscopy (SEM), transmission electron microscopy (TEM), high-resolution transmission electron microscopy (HRTEM), photoluminescence (PL), low voltage cathodoluminescence (CL) and time-resolved emission spectra as well as kinetic decays were used to characterize the resulting samples. SEM and TEM results indicate the as-formed precursor fibers and belts are smooth, and the as-prepared nanofibers and microbelts consist of nanoparticles. The doped rare-earth ions show their characteristic emission under ultraviolet excitation, i.e. Ce^{3+} $5d$–$4f$ and Tb^{3+} $^5D_4$–^7F_J ($J=6$–3) transitions, respectively. The energy transfer process from Ce^{3+} to Tb^{3+} in $LaPO_4$:Ce^{3+}, Tb^{3+} nanofibers was further studied by the time-resolved emission spectra. Under low-voltage electron beam excitation, $LaPO_4$:Ce^{3+}, Tb^{3+} microbelt phosphors have a higher intensity than that of nanofiber phosphors.

1. Introduction

Inorganic luminescent materials have found many practical applications in modern lighting and display fields, such as fluorescent lamps, cathode-ray tubes, field emission displays and plasma display panels [1]. Oxide materials represent a class of inorganic materials with technologically relevant properties that could be used in the production of displays, lamps, and sensors. Morphology of phosphors (shape and size of the powder particles) is one of the key parameters of their industrial application [2,3]. Improvement of the morphology control is of great interest and different ways are tried in order to achieve this aim [2–4]. In fact, size and shape of the phosphor particles have an important influence on the emission intensity and the efficiency of the device. One-dimensional (1D) structures, such as fibers, tubes, wires, rods and belts, have attracted great research interests [5–8] because of their potential to test fundamental quantum mechanic concepts [9] and to play a vital role in various applications such as photonics [10], nanoelectronics [11] and data storage [12]. Quasi-one-dimensional (Q-1D) nanostructures also have attracted intensive experimental and theoretical interests as a result of their novel physical properties and potential application [9,13,14]. As one subgroup of Q-1D nanostructures, nanobelts not only help to extend the understanding of the relationships between structure and property but can also contribute to an ideal system for building functional devices. Exploring nanobelts with very large widths on the micrometer, microbelts still remains significant on promising properties [15–17].

1D and Q-1D nanomaterials with different compositions have been developed using various methods [18–23] including the chemical or physical vapor deposition, laser ablation, solution, arc discharge, vapor-phase transport process, and a template based method. Compared to these, electrospinning is an effective and simple method for generating 1D materials with diameters ranging from 10's of nanometers up to micrometers. The electrospinning technique has been developed since 1934 for the synthesis of 1D materials [24] and now it is demonstrated that a rich variety of materials can be electrospun to form uniform 1D materials [25–31], such as polymers, inorganic and hybrid (organic–inorganic) compounds. On the other hand, the sol–gel process has been proven as an efficient way to produce nanoparticles [32] and nanocoatings [33] of metal oxide. Sol–gel techniques can be employed to prepare precursor solutions, which have been used to deposit coatings by spinning and dipping [34]. 1D materials fabricated by a combination method of sol-gel process and electrospinning have become important for their exceptionally long length, uniform diameter, diverse composition and high surface, which can be applied in biomedical fields, reinforced composites, catalyst supports, sensors, electronic and optical devices, as well as sacrificial templates [35–38].

Lanthanide orthophosphates ($LnPO_4$) belong to two polymorphic types, the monoclinic monazite type (for La to Gd) and

* Corresponding author. Fax: +86 431 85698041.
E-mail address: jlin@ciac.jl.cn (J. Lin).

0022-4596/$ - see front matter © 2008 Elsevier Inc. All rights reserved.
doi:10.1016/j.jssc.2008.12.021

Table 1
The summary of the experiment conditions and the corresponding morphologies.

Sample	Volume ratio water:ethanol	Type of PVP/wt% of PVP	Voltage (kV)/spinning rate (mL h^{-1})/distance (cm)	Morphology
$LaPO_4$:0.2Ce^{3+} $LaPO_4$:0.15Tb^{3+} $LaPO_4$:0.2Ce^{3+}, 0.15Tb^{3+}	1:4	M_w = 1,300,000, Aldrich/8 wt%	18/0.5/16	nanofiber
$LaPO_4$:0.2Ce^{3+} $LaPO_4$:0.15Tb^{3+} $LaPO_4$:0.2Ce^{3+}, 0.15Tb^{3+}	2:3	K-30, SCRC/25 wt%	25/1/16	microbelt

the quadratic xenotime type (for Tb to Lu). Lanthanum phosphate ($LaPO_4$, monazite) has been shown to be a useful host lattice for rare earth ions to produce phosphors emitting a variety of colors [39–43]. In comparison with bulk materials, the shape anisotropy of a 1D structure provided a better model system to investigate the dependence of electronic transport and optical properties on size confinement and dimensionality. Therefore, the luminescent $LaPO_4$:*RE* (rare earth) 1D nanocrystals have also attracted considerable interest [44–46]. Ce^{3+} and Tb^{3+} ions are important *RE* ions, which have been applied in blue and green phosphors. Ce^{3+} and Tb^{3+} coactivated $LaPO_4$ is a highly efficiently and commercially applied green ($^5D_4$–$^7F_5$ of Tb^{3+} at 543 nm) phosphor in fluorescent lamps [1]. As far as we know, no study has been reported on synthesis of 1D and Q-1D $LaPO_4$: Ce^{3+}, Tb^{3+} phosphor materials together with their luminescent properties via electrospinning process. Accordingly in this paper, we report the preparation of 1D fiberlike and Q-1D beltlike $LaPO_4$:Ce^{3+} and/or Tb^{3+} phosphors through a combination method of sol-gel process and electrospinning, as well as their photoluminescent and cathodoluminescent properties.

2. Experimental section

2.1. Chemicals and materials

Polyvinylpyrrolidone (PVP, M_w = 1,300,000) was purchased from Aldrich. Polyvinylpyrrolidone (PVP, K-30) was purchased from Sinopharm Chemical Reagent Co., Ltd. Ammounium biphosphate $(NH_4)H_2PO_4$ (⩾99.0%, analytical reagent, A. R.), citric acid monohydrate $C_6H_8O_7 \cdot H_2O$ (⩾99.5%, A. R.), nitric acid HNO_3 (A. R.) and ethanol were all purchased from Beijing Fine Chemical Company. La_2O_3 and Tb_4O_7 (99.99%) were purchased from Science and Technology Parent Company of Changchun Institute of Applied Chemistry. $Ce(NO_3)_3 \cdot 6H_2O$ (99.99%) was purchased from Shanghai Yuelong New Materials Co., LTD. $La(NO_3)_3$ was prepared by dissolving La_2O_3 in dilute nitric acid HNO_3 and $Tb(NO_3)_3$ were prepared by dissolving Tb_4O_7 in dilute nitric acid HNO_3 containing H_2O_2, then evaporating the water in the solutions by heating. All the initial chemicals in this work were used without further purification.

2.2. Preparation

Nanofibers of $LaPO_4$:0.2Ce^{3+} and/or 0.15Tb^{3+} phosphors were prepared by a method of sol-gel process and electrospinning. The stoichiometric amounts of $La(NO_3)_3$, $Tb(NO_3)_3$, $Ce(NO_3)_3 \cdot 6H_2O$ and $(NH_4)H_2PO_4$ were dissolved in deionized water and the pH value of the solution was kept between two and three by adding HNO_3. Then the solution was mixed with a water–ethanol solution (final volume ratio of water to ethanol is 1:4) containing citric acid as a chelating agent for the metal ions. The molar ratio of metal ions to citric acid was 1:2. A certain amount of polyvinylpyrrolidone (PVP, M_w = 1,300,000, Aldrich) was added to adjust the viscoelastic behavior of the solution (the weight percentage of PVP is 8% in the water–ethanol solution). The solution was stirred for 4 h to obtain a homogeneous hybrid sol for further electrospinning. The distance between the spinneret (a metallic needle) and collector (a grounded conductor) was fixed at 16 cm and the high-voltage supply was maintained at 18 kV. The spinning rate was controlled at 0.5 mL h^{-1} by a syringe pump (TJ-3A/W0109-1B, Baoding Longer Precision Pump Co., Ltd, China). The as-prepared hybrid precursor samples were to the desired temperature (600–900 °C) with the heating rate of 2 °C · min^{-1} and held there for 4 h in air. In a typical process for the preparation of $LaPO_4$:0.2Ce^{3+} and/or 0.15Tb^{3+} microbelts, the solution for electrospinning was prepared by the similar procedure via changing the ratio of water–ethanol solution together with the type and amount of PVP. Typically, the ratio of water–ethanol solution was adjusted to 2:3 in volume, another kind of polyvinylpyrrolidone (PVP, K-30, Sinopharm Chemical Reagent Co., Ltd) was added with a weight percentage of 25% in the water–ethanol solution. The solution was also stirred for 4 h to obtain a homogeneous hybrid sol for electrospinning. The distance between the spinneret and collector was tuned to 16 cm and the high-voltage supply was changed to 25 kV. The spinning rate was controlled at 1 mL h^{-1} by a syringe pump. The as-formed hybrid precursor samples were to the desired temperature (600–900 °C) with the heating rate of 2 °C · min^{-1} and maintained for 4 h in air. In this way, $LaPO_4$:0.2Ce^{3+} and/or 0.15Tb^{3+} nanofibers and microbelts have been prepared. The detailed sample synthesis parameters and compositions (including the doping concentrations in synthesis and actual concentrations determined by analysis) are summarized in Tables 1 and 2, respectively.

Table 2
Nominal and analyzed compositions of $LaPO_4$:*x* Ce^{3+}, *y* Tb^{3+} (analyzed by ICP-OES). Here *x* is the doping molar concentrations of Ce^{3+} and *y* is the doping molar concentrations of Tb^{3+}, NF: nanofibers, MB: microbelts.

Sample	*x* nominal	*x* analyzed	*y* nominal	*y* analyzed
$LaPO_4$:0.2Ce^{3+} (NF)	0.200	0.189	–	–
$LaPO_4$:0.15Tb^{3+} (NF)	–	–	0.150	0.141
$LaPO_4$:0.2Ce^{3+}, 0.15Tb^{3+} (NF)	0.200	0.191	0.150	0.139
$LaPO_4$:0.2Ce^{3+} (MB)	0.200	0.193	–	–
$LaPO_4$:0.15Tb^{3+} (MB)	–	–	0.150	0.145
$LaPO_4$:0.2Ce^{3+}, 0.15Tb^{3+} (MB)	0.200	0.195	0.150	0.137

2.3. Characterization

The powder X-ray diffraction (XRD) patterns of the samples were carried out using a Bruker-D8 Focus diffractometer with copper radiation (Cu$K\alpha$, 0.154056 nm). The powder XRD pattern

for Rietveld analysis were measured with a step (counting time: 2 s · step^{-1}) width of 0.02° in the 2θ range between 10 and 80°. The morphology of the samples was inspected using a field emission scanning electron microscope (Philips XL 30). Transmission electron microscopy (TEM) and high-resolution transmission electron microscopy (HRTEM) micrographs were obtained from a FEI Tecnai G2 S-Twin transmission electron microscope with a field emission gun operating at 200 kV. Inductively coupled plasma optical emission spectrometer (ICP-OES, ICAP 6300, Thermal Scientific) was used to determine the actual doping molar concentrations of Ce^{3+} and Tb^{3+} in $LaPO_4$:Ce^{3+} and/or $LaPO_4$:Tb^{3+} samples. The photoluminescence (PL) measurements were performed on a Hitachi F-4500 spectrophotometer equipped with a 150 W xenon lamp as the excitation source. The cathodoluminescence (CL) measurements were conducted in an ultrahigh-vacuum chamber ($<10^{-8}$ Torr), where the phosphors were excited by an electron beam at a voltage range of 1–3 kV with different filament currents 14–18 mA, and the emission spectra were recorded using an F-4500 spectrophotometer. The luminescence decay curves and time-resolved PL spectra were obtained from a Lecroy Wave Runner 6100 digital oscilloscope (1 GHz) using a tunable laser (pulse width = 4 ns, gate = 50 ns) as excitation (Continuum Sunlite OPO). All the measurements were performed at room temperature.

3. Results and discussion

3.1. Formation, structure and morphology

3.1.1. XRD

Fig. 1 shows the XRD patterns of the as-prepared precursor for $LaPO_4$:0.2Ce^{3+}, 0.15Tb^{3+} (fiberlike) sample, and those annealed from 600 to 900 °C as well as the JCPDS card (no. 32–0493) for $LaPO_4$, respectively. In Fig. 1(a) for the as-formed precursor sample, no diffraction peak is observed except for the broad band at 2θ = 22°, which is ascribed to the semicrystalline PVP. For the precursor sample annealed below 600 °C, the broad peak for semicrystalline PVP disappears and no diffraction peak is observed in the XRD pattern (not shown), indicating that the decomposition of PVP and the sample remains amorphous at this stage. When the precursor sample is calcined at 600 °C (Fig. 1b), some weak and broad peaks at 2θ = 21.58°, 27.35°, 28.65°, 30.95°, 42.16°, 45.65° are present, which are due to the (101), (200), (120), (012), (221), (312), reflections of the crystalline $LaPO_4$ (monazite structure), respectively. This indicates the starting of crystallization of the fiberlike sample at this heating temperature. With the increase of annealing temperature from 700 to 900 °C (Fig. 1c–e), the diffraction peaks become sharper and stronger due to the increase of the crystallinity and the growth of the crystallize size. For the sample annealed at 900 °C (Fig. 1e), well defined diffraction peaks can be indexed to the monoclinic phase of $LaPO_4$ according to the JCPDS card (no. 32–0493). No additional peaks for other phases have been found, indicating that Ce^{3+} and Tb^{3+} ions have been effectively built into the $LaPO_4$ host lattice and the doping degree cannot give rise to the change of the crystal phase. The same situation of XRD results holds for other Ce^{3+} and/or Tb^{3+} doped $LaPO_4$ samples (fiberlike and beltlike) obtained under other experimental conditions.

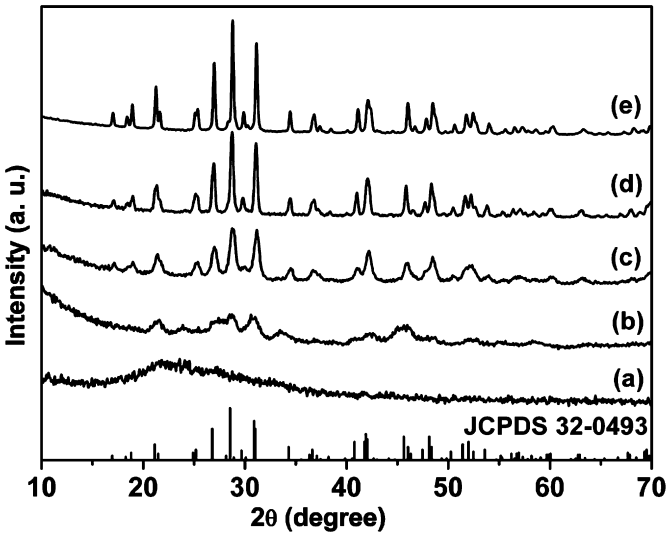

Fig. 1. X-ray diffraction patterns for $LaPO_4$:0.2Ce^{3+}, 0.15Tb^{3+} nanofibers, (a) as-form precursor fibers, the fibers annealed at (b) 600 °C, (c) 700 °C, (d) 800 °C and (e) 900 °C, respectively, as well as the JCPDS card 32–0493 of $LaPO_4$ for comparison.

$LaPO_4$:Ce^{3+}, Tb^{3+} samples have the space group $P2_1/n$, and the structure comprises numbers of PO_4 tetrahedra and REO_9 (RE = La, Ce and Tb) polyhedra [47,48]. The phosphate tetrahedra in the structure is isolated, separated by intervening REO_9 polyhedra, and O atoms in coordinate to two RE and one P atoms. The fundamental atomic arrangements of $LaPO_4$:Ce^{3+}, Tb^{3+} can be described as [001] chains formed of alternating RE polyhedra and phosphate tetrahedra (called polyhedron-tetrahedron chains). The chains extend along [001] by sharing tetrahedral edges with RE polyhedra; there are four chains per unit cell in each mineral. The chains are linked laterally [in (001)] by sharing edges of adjacent REO_9 polyhedra. The crystal structures of the as prepared Ce^{3+} and/or Tb^{3+} doped $LaPO_4$ samples (annealed at 900 °C) were refined by the Rietveld method [49,50]. The unit cell of $LaPO_4$:Ce^{3+}, Tb^{3+} was first determined from the X-ray powder diffraction patterns using indexing programs DICVOL04 [51] and the XRD data were analyzed by the Rietveld method using GSAS [52]. In the refinement, the first one was a profile matching step, introduced by LeBail [53]. Here unit cell parameters, profile shape parameters and the individual Bragg intensities varied independently without referring to any structural model. In the second stage of Rietveld analysis, we refined the position and fractional occupancy of the atoms, holding the unit cell and profile shape parameters obtained in the first step. Constraint has been used in the third step, where the occupancies of La and Ce/Tb were varied while the total occupancy of La and Ce/Tb was kept equal to the stoichiometric ratio. Finally, the occupation of Ce/Tb was refined for all samples. The diffraction patterns obtained can be successfully indexed and refined for all samples in the frame of the monoclinic space group $p2_1/n$. Fig. 2 shows the Rietveld refinement patterns using XRD data of as-prepared $LaPO_4$:0.2Ce^{3+}, 0.15Tb^{3+} microbelts (a) and nanofibers (b) (as examples). The calculated intensity agreed well with the observed data. The most important structural parameters and the discrepancy factors after the refinement are listed in Table 3, and the main interatomic distances and bond angles of $LaPO_4$:Ce^{3+}, Tb^{3+} nanofibers (as an example) are listed in Table 4. For example, for the $LaPO_4$:0.2Ce^{3+}, 0.15Tb^{3+} nanofibers, the reliability factors were R_{wp} = 5.23%, R_p = 1.682%, R_F^2 = 1.682% and χ^2 = 1.430, and the unit-cell parameters obtained were a = 6.81656(3) Å, b = 7.057175(4) Å, c = 6.49545(1) Å, $\alpha = \gamma = 90°$, and β = 103.357(2)° (Table 3). The calculated crystal cell parameters are smaller than those for the standard $LaPO_4$ (JCPDS 32–0493). The smaller cell parameters (a, b, c) are attributable to the smaller Ce and Tb atoms as compared with the La atoms. Ionic radii of the Ce^{3+} and Tb^{3+} ions (1.034 and 0.923 Å) are smaller than that of the La^{3+} ion (1.061 Å).

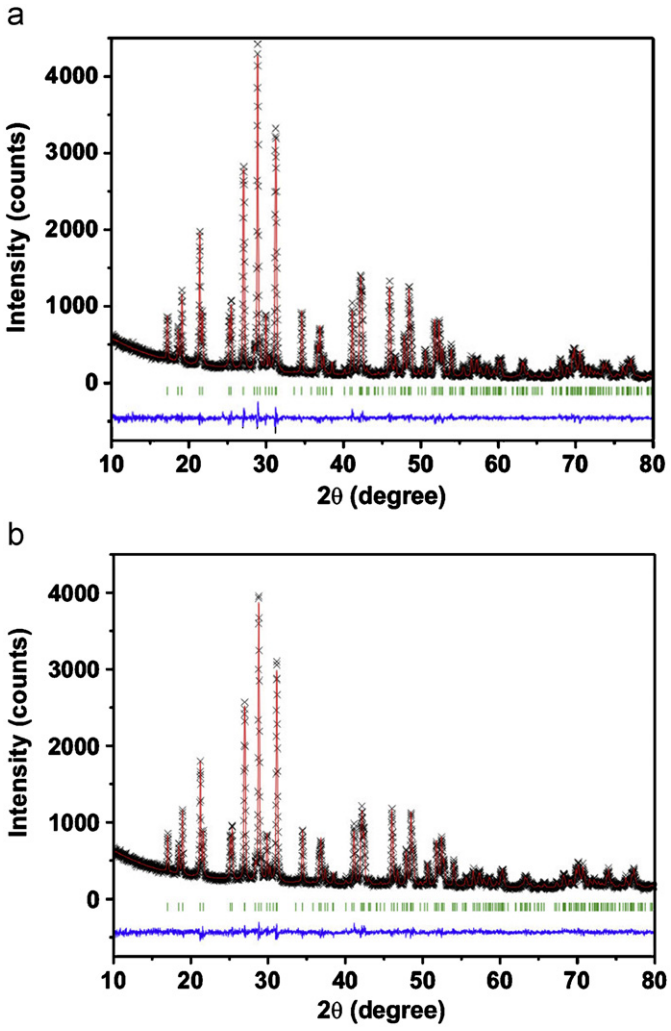

Fig. 2. The observed (black fork mark) and calculated (red solid) X-ray diffraction profiles of $LaPO_4$:$0.2Ce^{3+}$, $0.15Tb^{3+}$ microbelts (a) and nanofibers (b). The short vertical bars (green) show the positions of the allowed Bragg reflections. The difference profile (blue solid) is located at the bottom of the figures. (For interpretation of the references to colour in the figure legend, the reader is referred to the web version of the article).

3.1.2. SEM and TEM

Fig. 3 shows the SEM images of the as-formed precursor $LaPO_4$:$0.2Ce^{3+}$, $0.15Tb^{3+}$ hybrid fibers and belts, as well as those samples annealed at high temperature (900 °C), respectively. From the SEM micrograph of Fig. 3a, it can be seen that the as-formed $LaPO_4$:$0.2Ce^{3+}$, $0.15Tb^{3+}$ precursor fibers are uniform with diameters ranging from 150 to 300 nm. In order to obtain pure inorganic fibers, a high annealing temperature is employed to remove the organic PVP templates. After being calcined at 900 °C for 4 h, the fibers shrink and become curvy due to the decomposition of PVP and crystallization of $LaPO_4$. It can also be seen from Fig. 3b that the diameters of $LaPO_4$:$0.2Ce^{3+}$, $0.15Tb^{3+}$ nanofibers (seem to consist of linked particles) become 75–150 nm. The morphology and diameter of electrospun 1D nanomaterials are dependent on a number of processing parameters including the type of polymer, the conformation of polymer chain, electrical conductivity, the surface tension and the operational conditions. Under controlling these factors, the formation of a skin on the surface of liquid jet (due to rapid evaporation of solvent) and the subsequent collapse of the skin might be responsible for the emergence of a beltlike morphology [54–56]. Additionally, a higher flow rate for solution always leads to the formation of thicker fibers, and these thicker fibers without complete drying before reaching the collector may also lead to the formation of beltlike structures with rectangular cross sections [55,57]. By adjusting some of the electrospun parameters, we can obtain Q-1D hybrid beltlike materials, as shown in Fig. 3c. In general, the precursor belts are formed with typical widths of 0.5–2 μm and thickness of 200–500 nm. After annealed at 900 °C for 4 h, the sample keeps beltlike structure with widths of 0.3–1.5 μm and thickness in the range of 150–300 nm (Fig. 3d).

The morphologies of 1D and Q-1D products are further characterized by TEM and HRTEM techniques. The TEM and HRTEM images of $LaPO_4$:$0.2Ce^{3+}$, $0.15Tb^{3+}$ nanofibers and microbelts are shown in Fig. 4, respectively. From Fig. 4a and c, it can be seen that the nanofibers or microbelts are further composed of closely-linked nanoparticles. The typical HRTEM images of $LaPO_4$:$0.2Ce^{3+}$, $0.15Tb^{3+}$ nanofibers (Fig. 4b) and microbelts (Fig. 4d) clearly show lattice fringes with interplanar spacing of 0.31 nm that correspond to the (112) plane of $LaPO_4$, respectively. These results further confirm the presence of highly crystalline $LaPO_4$:$0.2Ce^{3+}$, $0.15Tb^{3+}$ in the nanofiber and microbelt samples after annealing at high temperature, agreeing well with the XRD results.

Finally, it should be mentioned that the key strategy of sol–gel/electrospinning method to obtain 1D inorganic nanomaterials was to form a solution with viscoelastic behavior similar to that of a conventional polymer solution. In our experiments, the purposes of controlling the volume ratio of water to alcohol and the weight percentage of PVP were to adjust the viscoelastic behavior, making the hybrid solution suitable for further electrospinning. The morphology and diameter of electrospun samples are also dependent on a number of process parameters including the intrinsic properties of solution and the operational conditions. In order to obtain uniform 1D morphologies, searching for a balance point of various electrospinning parameters is very important. In our experiments, the balance point might be related to the volume ratio of water to alcohol, the weight percentage of PVP, the spinning rate, the strength of electric field, and the distance between the spinneret and collector. The synthesis conditions listed in Table 1 are the optimized ones for the corresponding morphologies.

3.2. Luminescence properties

The PL and spectral properties for the Ce^{3+} and/or Tb^{3+} doped $LaPO_4$ nanofibers and microbelts are basically identical, so here we mainly present the results for the Ce^{3+} and/or Tb^{3+} doped $LaPO_4$ nanofibers.

3.2.1. PL properties of $LaPO_4$:Ce^{3+}/Tb^{3+} nanofibers

Under short wavelength ultraviolet (UV) irradiation, as-prepared $LaPO_4$:Tb^{3+} nanofibers exhibit green emission for Tb^{3+}. Fig. 5 shows the PL excitation and emission spectra of $LaPO_4$:$0.15Tb^{3+}$ nanofibers. The excitation spectrum (Fig. 5a) of Tb^{3+} contains an intense band at 216 nm with a shoulder at 230 nm, which are due to the transitions from the ground state ($^7F_6$) of the Tb^{3+} $4f^8$ configuration to the different excited states of the $4f^7$ $5d$ configuration. The forbidden f–f excited transitions of Tb^{3+} can not be observed clearly due to their weak intensity with respect to that of the allowed $4f^8$–$4f^7$ $5d$ transition. Excitation into the $4f^8$–$4f^7$ $5d$ band at 216 nm yields the characteristic green emission $^5D_4$–^7F_J ($J = 3, 4, 5, 6$) of Tb^{3+}, with the $^5D_4$–$^7F_5$ (543 nm) green emission as the most prominent group (Fig. 5b). Due to the cross-relaxation between $^5D_3$–$^5D_4$ and $^7F_0$–$^7F_6$ at this high doping

Table 3
Structure parameters for $LaPO_4$: xCe^{3+}, yTb^{3+} nanofibers and microbelts. (RE: La/Ce/Tb).

	$x=0.15$, $y=0$ nanofiber	$x=0.15$, $y=0$ microbelt	$x=0$, $y=0.2$ nanofiber	$x=0$, $y=0.2$ microbelt	$x=0.15$, $y=0.2$ nanofiber	$x=0.15$, $y=0.2$ microbelt
Unit cell parameters						
a (Å)	6.82814(1)	6.82821(1)	6.82653(4)	6.82651(6)	6.81656(3)	6.81689(3)
b (Å)	7.06114(5)	7.06086(2)	7.05615(2)	7.05631(7)	7.05175(4)	7.05206(5)
c (Å)	6.50125(2)	6.50065(1)	6.50049(2)	6.50048(5)	6.49545(1)	6.49583(1)
$\alpha=\gamma$ (deg)	90	90	90	90	90	90
β (deg)	103.297(3)	103.289(1)	103.344(5)	103.343(6)	103.357(2)	103.362(1)
Reliability factors						
R_{wp} (%)	9.17	9.12	9.38	9.33	6.82	5.07
R_p (%)	6.35	6.45	7.12	7.09	5.23	4.53
R_F^2 (%)	2.216	3.659	2.968	4.265	1.682	2.134
χ^2	2.368	2.071	3.256	3.569	1.430	1.331
Atomic positions						
RE						
x	0.2833(2)	0.2835(3)	0.2828(6)	0.2829(7)	0.2829(3)	0.2837(2)
y	0.1603(0)	0.1606(1)	0.1598(7)	0.1598(5)	0.1601(5)	0.1599(0)
z	0.1010(5)	0.1006(0)	0.0998(1)	0.0999(1)	0.1005(3)	0.0997(8)
Uiso (Å^2)	0.0196(1)	0.0231(6)	0.0311(4)	0.0177(1)	0.0335(0)	0.0222(6)
P						
x	0.3037(4)	0.3029(2)	0.3022(6)	0.3022(7)	0.3038(0)	0.3041(0)
y	0.1613(1)	0.1622(1)	0.1623(9)	0.1614(5)	0.1634(2)	0.1629(8)
z	0.6097(2)	0.6077(1)	0.6049(7)	0.6074(3)	0.6114(9)	0.6112(5)
Uiso (Å^2)	0.0156(4)	0.0301(2)	0.0255(0)	0.0217(4)	0.0206(7)	0.0206(9)
O_1						
x	0.2515(3)	0.2492(3)	0.2497(3)	0.2503(5)	0.2510(1)	0.2508(5)
y	0.0089(7)	0.0086(2)	0.0085(6)	0.0083(0)	0.0086(1)	0.0088(6)
z	0.4460(5)	0.4466(3)	0.4456(7)	0.4459(8)	0.4462(3)	0.4461(2)
Uiso (Å^2)	0.0123(5)	0.0213(6)	0.0095(2)	0.0075(8)	0.0156(2)	0.0042(7)
O_2						
x	0.3796(1)	0.3855(1)	0.3817(4)	0.3817(4)	0.3802(7)	0.3801(2)
y	0.3314(5)	0.3313(4)	0.3354(2)	0.3360(9)	0.3313(2)	0.3315(3)
z	0.4494(3)	0.4984(5)	0.4976(7)	0.4980(4)	0.4967(2)	0.4975(0)
Uiso (Å^2)	0.0096(7)	0.0098(8)	0.0087(7)	0.0103(6)	0.0063(7)	0.0017(8)
O_3						
x	0.4737(0)	0.4740(1)	0.4742(7)	0.4736(5)	0.4741(4)	0.4735(1)
y	0.1066(3)	0.1060(5)	0.1073(0)	0.1064(6)	0.1069(1)	0.1063(8)
z	0.8050(2)	0.8042(0)	0.8027(9)	0.8033(1)	0.8029(2)	0.8031(1)
Uiso (Å^2)	0.0275(7)	0.0244(0)	0.0255(1)	0.02517(5)	0.0213(1)	0.0179(1)
O_4						
x	0.1268(2)	0.1272(1)	0.1270(1)	0.1276(3)	0.1269(2)	0.1274(3)
y	0.2153(4)	0.2156(6)	0.2152(2)	0.2156(6)	0.2153(1)	0.2165(3)
z	0.7125(0)	0.7131(5)	0.7120(7)	0.7122(0)	0.7112(5)	0.7117(2)
Uiso (Å^2)	0.0091(5)	0.0098(0)	0.0095(6)	0.0135(1)	0.0096(7)	0.0121(5)

concentration (15 mol%) of Tb^{3+}, the blue emission of the $^5D_3$–^7F_K transitions is too weak to be detected [1].

Ce^{3+} doped $LaPO_4$ nanofibers show an emission in the UV region. Fig. 6 gives the excitation and emission spectra, respectively, for the luminescence of $LaPO_4$:0.2Ce^{3+} nanofiber samples. The emission of Ce^{3+} includes a broad band with a maximum at 318 nm and a shoulder at 336 nm, which are assigned to the parity allowed transitions of the lowest component of the ^2D state to the spin-orbit components of the ground state, $^2F_{5/2}$, $^2F_{7/2}$ of Ce^{3+}, respectively. The energy difference between the two peaks is

1685 cm^{-1}, basically agreeing with the ground state splitting of Ce^{3+} (2000 cm^{-1}, i.e., energy difference between the $^2F_{5/2}$ and $^2F_{7/2}$ doublets in the $4f^1$ configuration of the Ce^{3+} ion). Independent of the monitored emission wavelengths (318 or 336 nm), the excitation spectrum consists of four broad peaks with maxima at 221, 245, 260, and 278 nm (strongest), which correspond to the transitions from the ground state $^2F_{5/2}$ of Ce^{3+} to the different components of the excited Ce^{3+} 5*d* states split by the crystal field (in the $LaPO_4$ host lattice, the La^{3+} ion is surrounded by nine oxygen atoms with a site symmetry of C_1 [43]). The intensity patterns and the positions of the peaks are in agreement with those observed in the absorption and luminescence excitation spectra of the bulk $LaPO_4$:Ce^{3+} and colloid of $LaPO_4$:Ce^{3+} nanocrystals [58–61].

3.2.2. PL properties of $LaPO_4$:Ce^{3+}, Tb^3 nanofibers

If the $LaPO_4$ nanofibers are coped with cerium and terbium ions, they show strong green luminescence under UV excitation caused by the line emission of Tb^{3+} ion. Fig. 7 exhibits the excitation and emission spectra for the luminescence of Tb^{3+} in $LaPO_4$:$0.2Ce^{3+}$, $0.15Tb^{3+}$ nanofiber phosphors. The excitation spectrum monitored with the 543 nm emission ($^5D_4$–$^7F_5$) of Tb^{3+} is composed exclusively of the excitation bands of Ce^{3+}, which is similar to the excitation spectrum of $LaPO_4$:$0.2Ce^{3+}$ (Fig. 6a). Excitation into the Ce^{3+} band at 278 nm yields both the weak emission of Ce^{3+} (300–360 nm) and the strong emission of Tb^{3+} (370–700 nm, $^5D_4$–^7F_J, $J = 3, 4, 5, 6$). This indicates that an energy transfer from Ce^{3+} to Tb^{3+} occurs in the nanofibers of $LaPO_4$, as observed in the bulk powder materials and colloids of $LaPO_4$:Ce^{3+}, Tb^{3+} [58–61]. All the above spectral properties for the $LaPO_4$:$0.2Ce^{3+}$, $0.15Tb^{3+}$ nanofiber phosphors are basically consistent with the reported bulk, nanocrystalline powder and thin film of $LaPO_4$:Ce^{3+}, Tb^{3+} [58–61]. The kinetic decay curves for the representative emission of Tb^{3+} and Ce^{3+} in $LaPO_4$:$0.2Ce^{3+}$, $0.15Tb^{3+}$ nanofibers and microbelts were measured, as shown in Figs. 8 and 9, respectively. The decay curves of Tb^{3+} $^5D_4$–$^7F_5$ (543 nm) luminescence can be well fitted to a single exponential function,

$$I = I_0 \exp(-t/\pi) \quad (1)$$

where I_0 is the initial emission intensity at $t = 0$, and t is the $1/e$ lifetime of the emission center. Through this fitting, the lifetimes of Tb^{3+} are determined to be 2.83 and 2.80 ms in nanofibers and microbelts (Fig. 8), respectively. Note that the lifetime values for Tb^{3+} in the $LaPO_4$:$0.2Ce^{3+}$, $0.15Tb^{3+}$ nanofibers and microbelts are basically identical within the experimental errors, which are close to that for Tb^{3+} in $La_{0.84}Tb_{0.16}PO_4$ thin film (2.78 ms, 900 °C annealed) [43]. Here the differences for the lifetimes of Tb^{3+} can be ascribed to the different composition and morphology of the samples. The luminescence decay curve for the representative emission of Ce^{3+} in $LaPO_4$:$0.2Ce^{3+}$, $0.15Tb^{3+}$ nanofibers and microbelts (Fig. 9) can also be fitted to a single exponential function, and the lifetimes of Ce^{3+} are also basically identical as Tb^{3+} in the nanofibers and microbelts, 5.95 and 5.92 ns, respectively.

The strong luminescence of Tb^{3+} results from efficient energy transfer from the Ce^{3+} to the Tb^{3+} in the $LaPO_4$:Ce^{3+}, Tb^{3+} phosphors, as reported previously [43,58–61]. In order to obtain more information about the energy transfer process from the Ce^{3+}

Table 4
Selected interatomic distances (Å) and bond angles (deg) for $LaPO_4$:$0.2Ce^{3+}$, $0.15Tb^{3+}$ nanofibers. (*RE*: La/Ce/Tb).

Interatomic distances (Å)			
Atoms	Distance	Atoms	Distance
RE–O1	2.5461(1)	*RE*–O2	2.7569(1)
RE–O1′	2.4748(5)	*RE*–O2′	2.5702(9)
		RE–O2″	2.6590(8)
RE–O3	2.5748(1)	*RE*–O4	2.4693(5)
RE–O3′	2.5007(6)	*RE*–O4′	2.5565(5)
P–O1	1.5279(6)	P–O2	1.5778(4)
P–O3	1.5293(2)	P–O4	1.5397(0)
Bond angle (deg)			
Bond type	Angle (deg)	Bond type	Angle (deg)
O1–P–O2	101.855(2)	O2–P–O3	106.655(2)
O1–P–O3	114.463(2)	O2–P–O4	117.642(1)
O1–P–O4	115.809(1)	O3–P–O4	100.629(2)

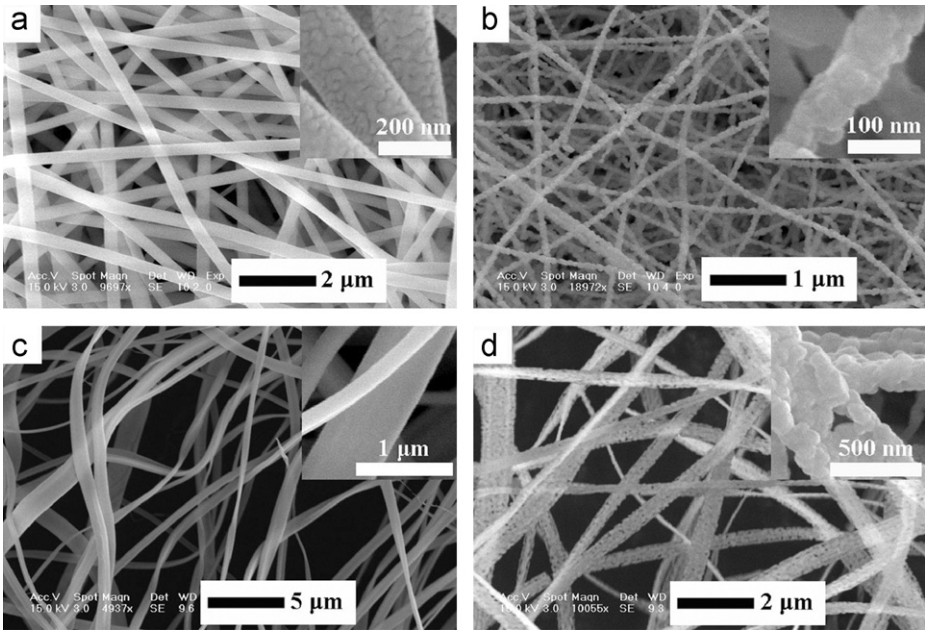

Fig. 3. SEM images for the as-formed precursor for $LaPO_4$ $0.2Ce^{3+}$, $0.15Tb^{3+}$ fiber (a) and that annealed at 900 °C (b), the as-formed precursor for $LaPO_4$:$0.2Ce^{3+}$, $0.15Tb^{3+}$ belts (c) and that annealed at 900 °C (d).

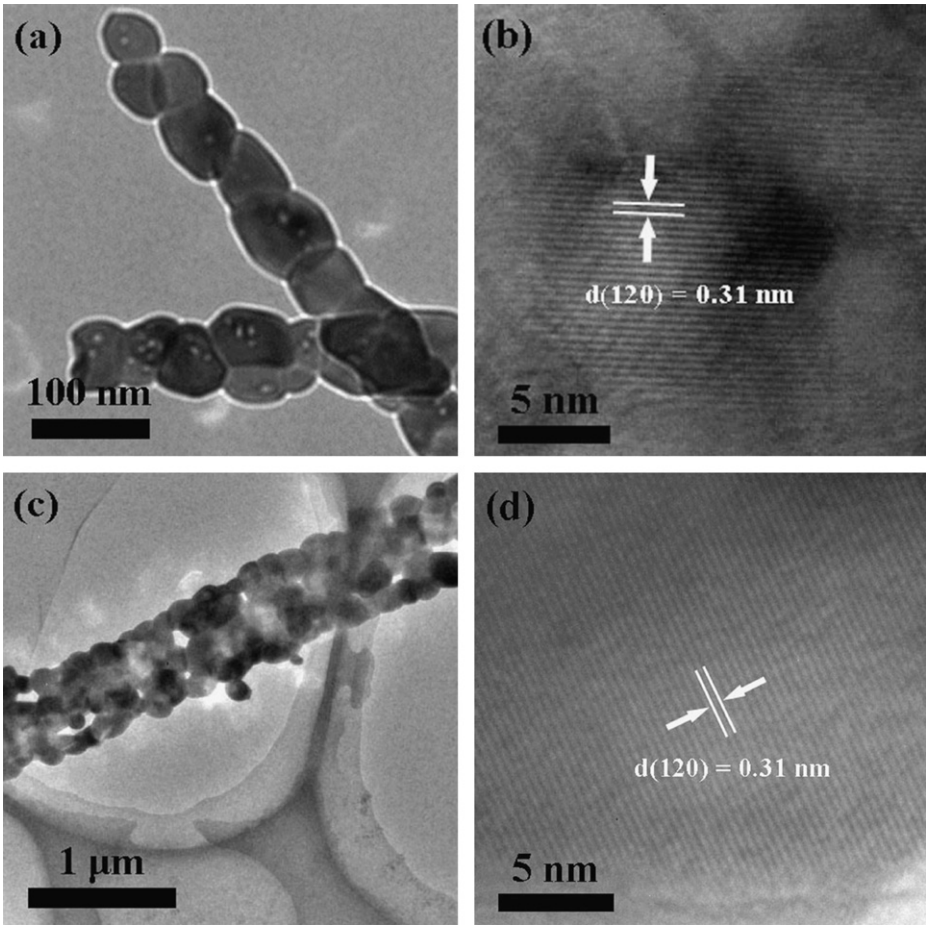

Fig. 4. TEM images of $LaPO_4$:0.2Ce^{3+}, 0.15Tb^{3+} nanofibers (a) with its HRTEM (b), $LaPO_4$:0.2Ce^{3+}, 0.15Tb^{3+} microbelts (c) with its HRTEM (d).

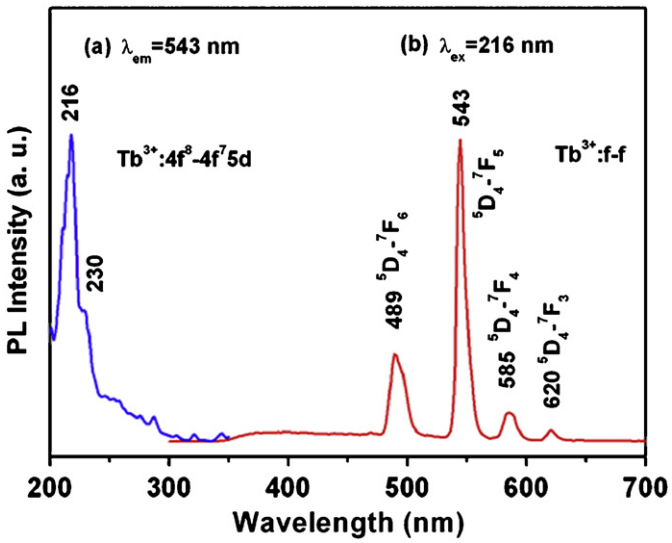

Fig. 5. Excitation (a) and emission (b) spectra for $LaPO_4$:0.15Tb^{3+} nanofibers.

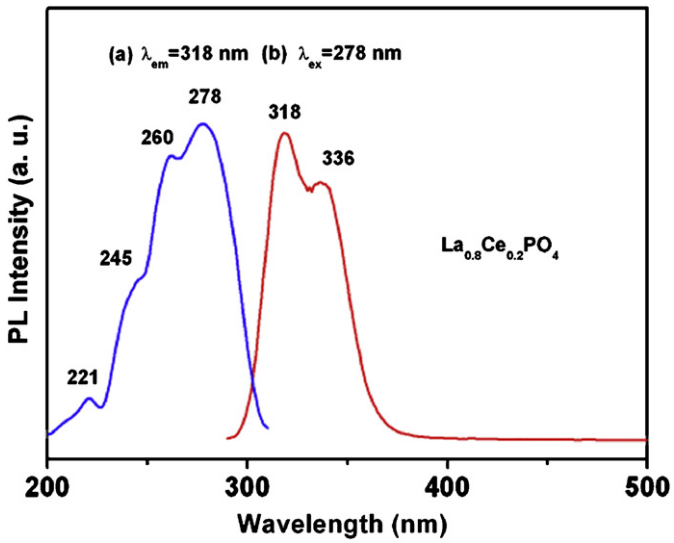

Fig. 6. Excitation (a) and emission (b) spectra for $LaPO_4$:0.2Ce^{3+} nanofibers.

to the Tb^{3+}, time-resolved emission spectra of Tb^{3+} in the $LaPO_4$:0.2Ce^{3+}, 0.15Tb^{3+} nanofiber phosphors were recorded at room temperature by exciting into the absorption of Ce^{3+} using a 290 nm laser with a delay time ranging from 0.05 to 100 μs, as shown in Fig. 10. When $t = 0.05$ μs, the broadband emission of Ce^{3+}, together with the weak emission of Tb^{3+} from $^5D_3$–^7F_J ($J = 6$, 5, 4, 3, 2), can be observed simultaneously, indicating that two processes occur in the excited Ce^{3+}: radiative transition to its ground state and nonradiative transfer of the excitation energy to the Tb^{3+} (mainly to high levels: $^5D_3$, $^5L_{10}$ at around 26 300 cm^{-1} (378 nm)). The competition between these two processes results in both the Ce^{3+} emission and the Tb^{3+} emission (mainly directly

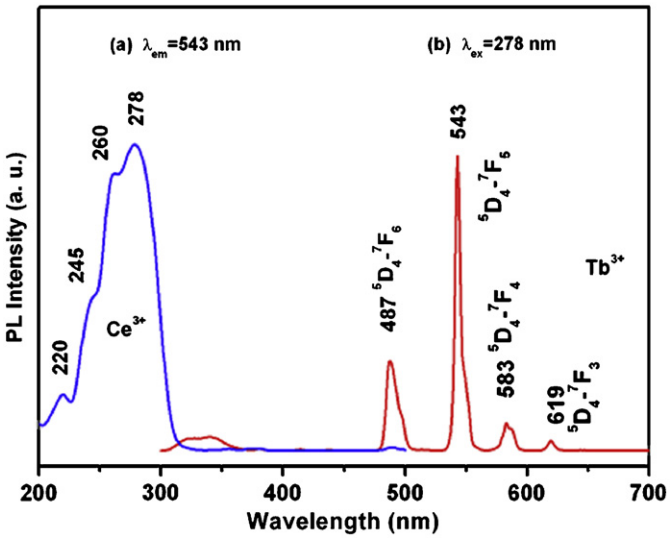

Fig. 7. Excitation (a) and emission (b) spectra for $LaPO_4$:0.2Ce^{3+}, 0.15Tb^{3+} nanofibers.

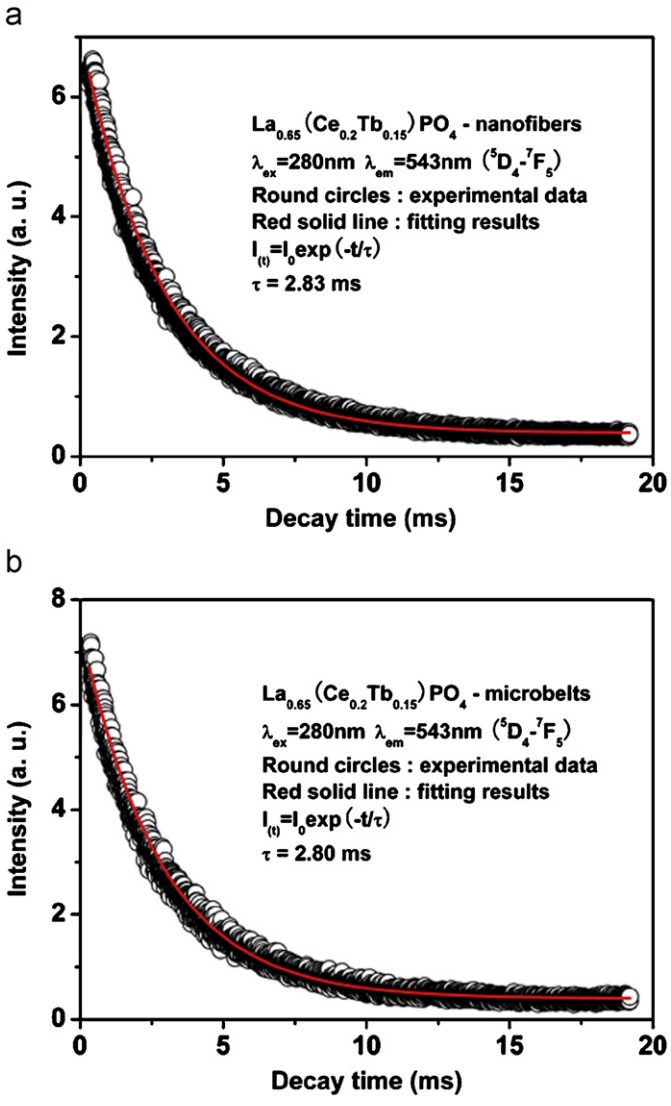

Fig. 8. The decay curves for the $^5D_4$–$^7F_5$ (543 nm) emission of Tb^{3+} in $LaPO_4$:0.2 Ce^{3+}, 0.15Tb^{3+} nanofibers (a) and microbelts (b).

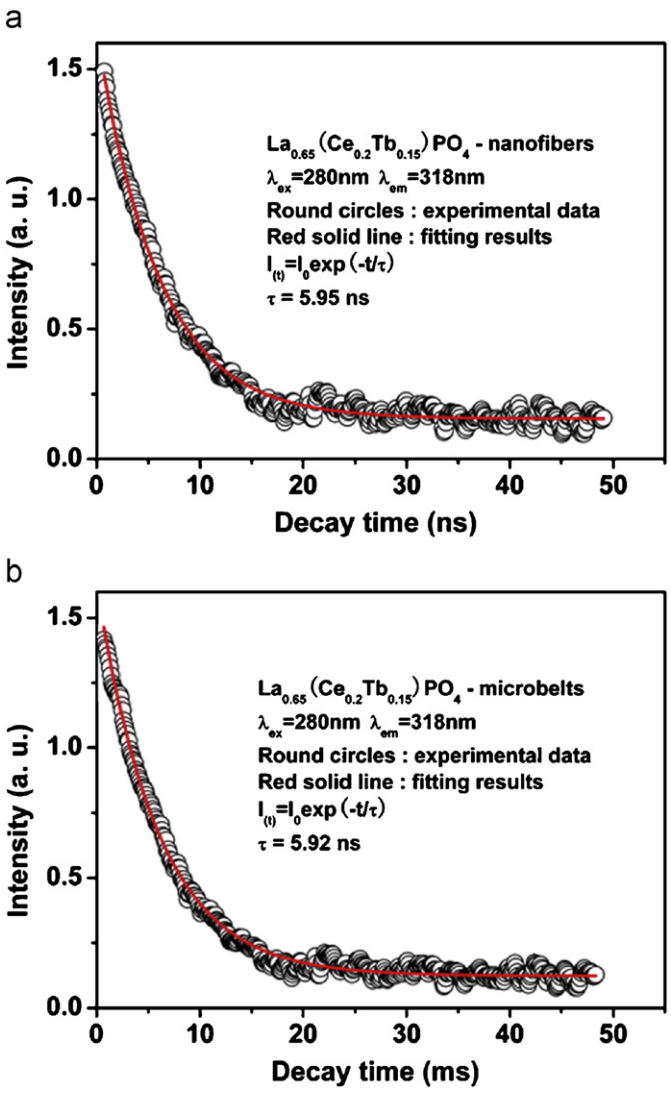

Fig. 9. The decay curves for Ce^{3+} in $LaPO_4$:0.2 Ce^{3+}, 0.15Tb^{3+} nanofibers (a) and microbelts (b).

from the $^5D_3$ level). When $t = 0.2\,\mu s$, $^5D_3$ excited states can be observed clearly and the emission of Ce^{3+} begins to decrease. When $t = 0.5\,\mu s$, the emission of Ce^{3+} cannot be observed due to its short lifetime ($\tau = 5.95$ ns depopulation takes place very quickly), and the $^5D_4$–^7F_J ($J = 6, 5, 4, 3$) emission of Tb^{3+} became dominant due to the cross-relaxation effect among the Tb^{3+} ions, i.e. Tb^{3+} ($^5D_3$)+Tb^{3+} ($^7F_6$) → Tb^{3+} ($^5D_4$)+Tb^{3+} ($^7F_0$) [43]. For $t = 10\,\mu s$ and later, the $^5D_3$ emission of Tb^{3+} is quenched completely by the cross-relaxation effect, and the $^5D_4$ emission also begins to decay gradually due to the depopulation of the excited states. Because the $^5D_4$ emission of Tb^{3+} has a lifetime of 2.83 ms (2830 μs), it can still be clearly observed for $t = 2000\,\mu s$ (figures are not shown due to the limited space). The luminescence and energy transfer process of Ce^{3+} and Tb^{3+} in $LaPO_4$:Ce^{3+}, Tb^{3+} is shown schematically in Fig. 11 [58,62]. First, Ce^{3+} ions were excited by UV light excitation; subsequently, energy transfer takes place from Ce^{3+} to Ce^{3+}, and then from 5*d* (Ce^{3+}) to the high excitation levels of Tb^{3+} ($4f^n$) followed by cross relaxation to the $^5D_4$ level of Tb^{3+}, which decays radiatively to various lower levels of ^7F_J ($J = 0, 1, 2, 3, 4, 5$ and 6). The energy levels of Tb^{3+} ($4f^n$) are suitable for the energy transfer to take place from the allowed Ce^{3+} emission (*f*–*d*) upon excitation with UV light. That the

Ce^{3+}–Ce^{3+} energy diffusion process should play a role in the energy transfer process appears reasonable in view of the involvement of parity-allowed *d–f* transition moments [58–61]. The Tb^{3+} ions act as the terminal of the energy transfer processes in the $LaPO_4$: Ce^{3+}, Tb^{3+} system.

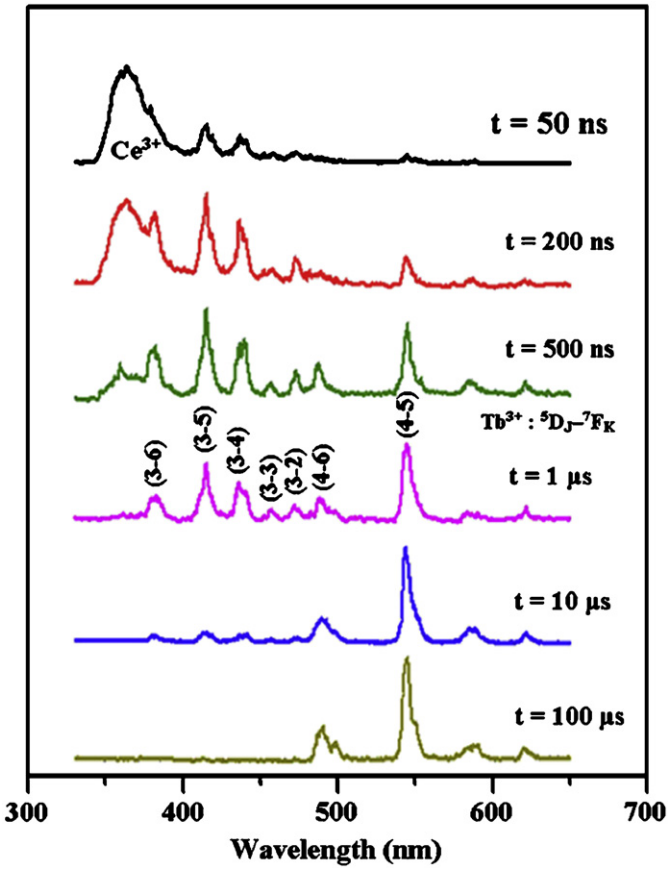

Fig. 10. Time-resolved emission spectra for the $LaPO_4$:0.2Ce^{3+}, 0.15Tb^{3+} nanofibers (λ_{ex} = 290 nm, laser).

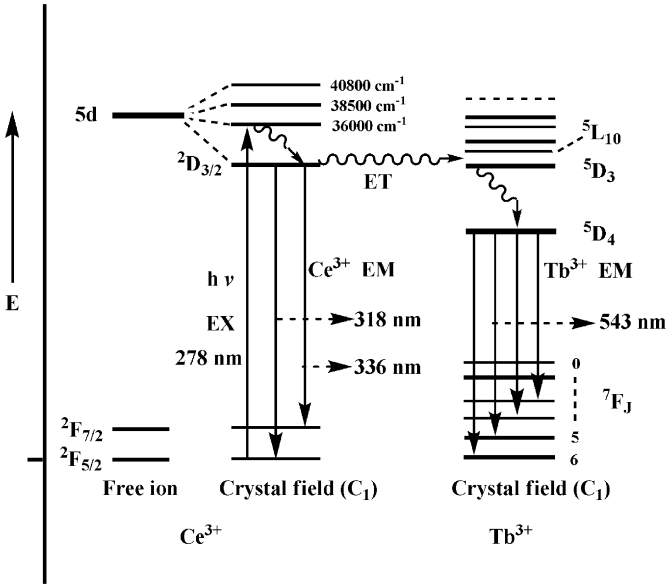

Fig. 11. The luminescence and energy transfer process of Ce^{3+} and Tb^{3+} in $LaPO_4$:0.2Ce^{3+}, 0.15Tb^{3+} nanofibers.

3.2.3. CL properties

Under low-voltage electron beam excitation, the as-prepared $LaPO_4$:0.2Ce^{3+}, 0.15Tb^{3+} microbelts and nanofibers also exhibit green emissions as the UV excitation, respectively. The representative cathodoluminescence spectra of the $LaPO_4$:0.2Ce^{3+}, 0.15Tb^{3+} microbelts and nanofibers under the excitation of electron beam (accelerating voltage = 1.5 kV; filament current = 15 mA) are

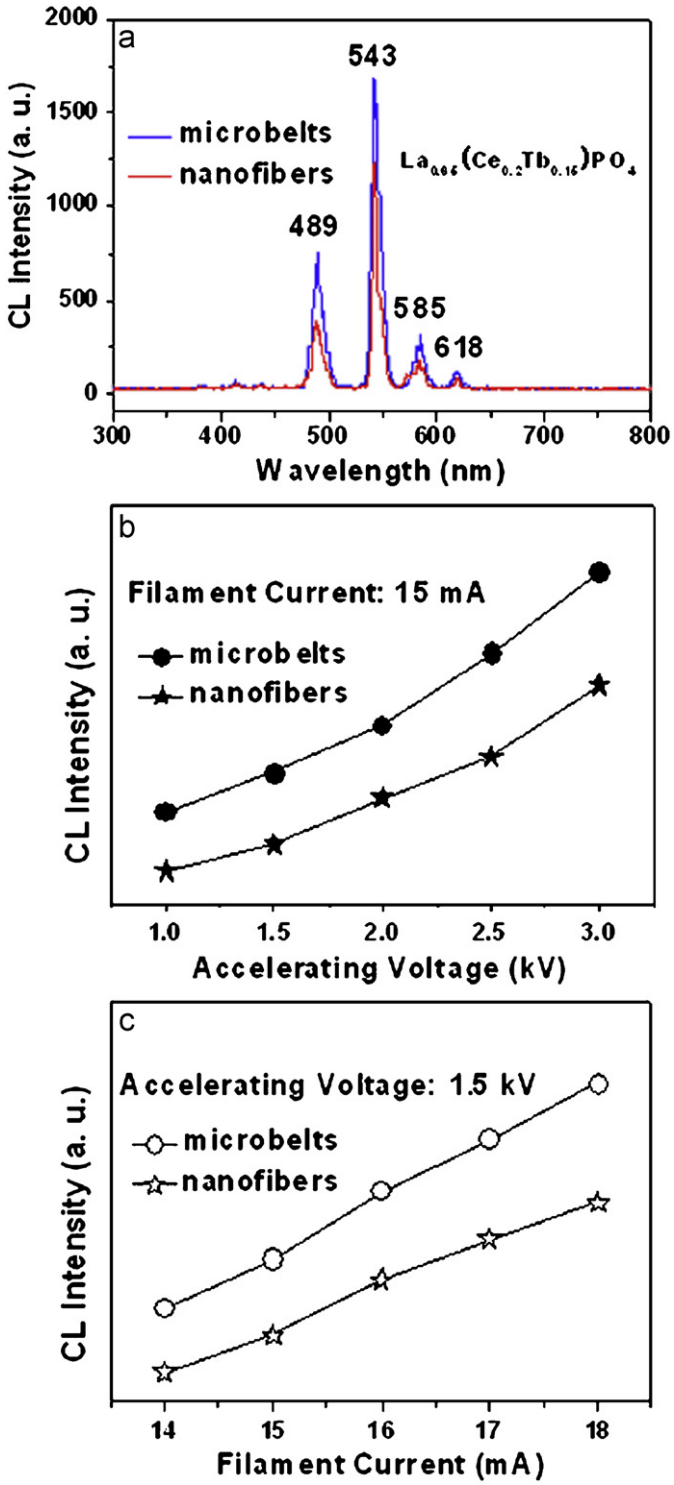

Fig. 12. Typical cathodoluminescence spectra (a) of $LaPO_4$:0.2Ce^{3+}, 0.15Tb^{3+} nanofibers and microbelts (acclelerating Voltage: 1.5 kV, Filament Current: 15 mA), the cathodoluminescence intensity of $LaPO_4$:0.2Ce^{3+}, 0.15Tb^{3+} nanofibers and microbelts as a function of accelerating voltage (b) and filament current (c).

shown in Fig. 12a, which have identical shapes as the PL emission spectra. From the typital CL spectra, it can be seen that the microbelts phosphors have a higher CL intensity than that of nanofibers phosphors (All the experimental conditions were kept identical in order to avoid experimental errors.) Defects have serious drawback in luminescence intensity for phosphors as they provide non-radiative recombination routes for electrons and holes [63–65]. From the HRTEM images shown in Fig. 4, it is clear that $LaPO_4$:0.2Ce^{3+}, 0.15Tb^{3+} nanofibers have a number of defect regions (Fig. 4b) and no obvious defects are found within the crystal structure of $LaPO_4$:0.2Ce^{3+}, 0.15Tb^{3+} microbelts (Fig. 4d). The large surface area introduces a large number of defects into the phosphor crystal. Herein, the surface area of the as-prepared $LaPO_4$:0.2Ce^{3+}, 0.15Tb^{3+} microbelts is smaller than that of $LaPO_4$:0.2Ce^{3+}, 0.15Tb^{3+} nanofibers. This is the reason that the CL intensity of microbelts is higher than that of nanofibers. The CL emission intensity for the $LaPO_4$:0.2Ce^{3+}, 0.15Tb^{3+} microbelt and nanofiber phosphors have been investigated as a function of the filament current and the accelerating voltage, as shown in Fig. 12, respectively. The CL intensity increased with the accelerating voltage from 1 to 3 kV (Fig. 12b). Similarly, when the accelerating voltage is fixed at 1.5 kV, the CL intensity also increases with raising the filament current from 14 to 18 mA (Fig. 12c). The increase in CL brightness with an increasing electron energy and filament current can be attributed to deeper penetration of electrons into the phosphors and the larger electron beam current density. The electron penetration depth can be estimated using the empirical formula,

$$L[\text{Å}] = 250(A/\rho)(E/Z^{1/2})^n \quad (2)$$

where $n = 1.2/(1-0.29\log_{10} Z)$, A is the atomic or molecular weight of the material, ρ is the bulk density, Z is the atomic number or the number of electrons per molecule in the case compounds, and E is the accelerating voltage (kV) [66]. For CL, the Ce^{3+}, Tb^{3+} ions are excited by the plasma produced by the incident electrons. The deeper the electron penetration depth, the more the plasmons will be produced, which resulted in more Ce^{3+}, Tb^{3+} ions being excited and thus the CL intensity increased.

4. Conclusions

In summary, Ce^{3+} and/or Tb^{3+} doped $LaPO_4$ one-dimensional nanofibers and quasi-one-dimensional microbelts have been successfully synthesized by means of electrospinning technique in conjunction with sol–gel process. The as-formed hybrid precursor materials present uniform fiberlike and beltlike morphologies. After annealing the precursors at high temperature, the as-prepared Ce^{3+} and/or Tb^{3+} doped $LaPO_4$ samples are well crystallized with fiber and belt morphologies compose of nanoparticles. The spectral and kinetic properties of the as-prepared Ce^{3+} and/or Tb^{3+} doped $LaPO_4$ phosphors have been investigated in detail. Under low-voltage electron beam excitation, microbelt phosphors have a higher CL intensity than the nanofiber phosphors due to lower defect concentration in the former. These studies indicate that a facile route for the development 1D and Q-1D luminescent nanomaterials that are useful in many types of color display fields.

Acknowledgments

This project is financially supported by National Basic Research Program of China (2007CB935502), and the National Natural Science Foundation of China (NSFC 50702057, 50872131, 00610227).

References

[1] G. Blasse, B.C. Grabmaier, Luminescent Materials, Springer, Heidelberg, Berlin, 1994.
[2] S. Oshion, K. Kitamura, T. Shigeta, S. Horii, T. Matsuoka, S. Tanaka, H. Kobayashi, J. Electrochem. Soc. 146 (1999) 392–399.
[3] Y.C. Kang, E.J. Kim, D.Y. Lee, H.D. Park, J. Alloys Compd. 347 (2002) 266–270.
[4] I.W. Lenggoro, B. Xia, H. Mizushima, K. Okuyama, N. Kijima, Mater. Lett. 50 (2001) 92–96.
[5] Y. Xia, P. Yang, Y. Sun, Y. Wu, B. Gates, Y. Yin, F. Kim, H. Yan, Adv. Mater. 15 (2003) 353–389.
[6] M. Bockrath, W. Liang, D. Bozovic, J.H. Hafner, C.M. Lieber, M. Tinkham, H. Park, Science 291 (2001) 283–285.
[7] Y. Huang, X.F. Quan, Q.Q. Wei, C.M. Lieber, Science 291 (2001) 851–853.
[8] D. Li, Y. Xia, Nanoletters 3 (2003) 555–560.
[9] J. Hu, T.W. Odom, C.M. Lieber, Acc. Chem. Res. 32 (1999) 435–445.
[10] S. Nakamura, Science 281 (1998) 956–961.
[11] C.A. Mirkin, Science 286 (1999) 2095–2096.
[12] R. O'Barr, S.Y. Yamamoto, S. Schultz, W.H. Xu, A. Scherer, J. Appl. Phys. 81 (1997) 4730–4732.
[13] A.P. Alivisator, Science 271 (1996) 933–937.
[14] E.W. Wong, P.E. Sheehan, C.M. Lieber, Science 277 (1997) 1971–1975.
[15] G.Z. Shen, J.H. Cho, J.K. Yoo, G.C. Yi, C.J. Lee, J. Phys. Chem. B 109 (2005) 9294–9298.
[16] J. Zhang, F.H. Jiang, Y.D. Yang, J.P. Li, J. Phys. Chem. B 109 (2005) 13143–13147.
[17] Y. Zhao, X. Zhu, Y.Y. Huang, S.X. Wang, J.L. Yang, Y. Xie, J. Phys. Chem. C 111 (2007) 12145–12148.
[18] S.Y. Bae, H.W. Seo, J. Park, H. Yang, J.C. Park, S.Y. Lee, Appl. Phys. Lett. 81 (2002) 126–128.
[19] L. Fu, Y.Q. Liu, P. Hu, K. Xiao, G. Yu, D.B. Zhu, Chem. Mater. 15 (2003) 4287–4291.
[20] X.F. Duan, C.M. Lieber, Adv. Mater. 12 (2000) 298–302.
[21] J.H. Jung, H. Kobayashi, B. Van, S. Shinkai, T. Shimizu, Chem. Mater. 14 (2002) 1445–1447.
[22] Y. Wu, P. Yang, Chem. Mater. 12 (2000) 605–607.
[23] M.H. Huang, A. Choudrey, P. Yang, Chem. Commun. 12 (2000) 1063–1064.
[24] A. Formhals, US Patent Specification, 1 975 504 (1934).
[25] S. Madhugiri, A. Dalton, J. Gutierrez, J.P. Ferraris, J. Kenneth, J. Balkus, J. Am. Chem. Soc. 125 (2003) 14531–14538.
[26] L. Yao, T.W. Haas, A. Guiseppi-Elie, G.L. Bowlin, D.G. Simpson, G.E. Wnek, Chem. Mater. 15 (2003) 1860–1864.
[27] G. Larsen, R. Velarde-Ortiz, K. Minchow, A. Barrero, I.G. Loscertales, J. Am. Chem. Soc. 125 (2003) 1154–1155.
[28] H.Q. Hou, D.H. Reneker, Adv. Mater. 16 (2004) 69–73.
[29] J. Wu, J.L. Coffer, Chem. Mater. 19 (2007) 6266–6276.
[30] J.J. Ge, H. Hou, Q. Li, M.J. Graham, A. Greiner, D.H. Reneker, F.W. Harris, Z.D. Cheng, J. Am. Chem. Soc. 126 (2004) 15754–15761.
[31] M.J. Li, J.H. Zhang, H. Zhang, Y.F. Liu, C.L. Wang, X. Xu, Y. Tang, B. Yang, Adv. Funct. Mater. 17 (2007) 3650–3656.
[32] P. Yang, M.K. Lu, C.F. Song, G.J. Zhou, D. Xu, D.R. Yuan, J. Phys. Chem. Solids 63 (2002) 2047–2051.
[33] X.A. Fu, S. Qutubuddin, Colloid Surf. A 186 (2001) 245–250.
[34] J.W. Zhai, L.Y. Zhang, X. Yao, S.N.B. Hodgson, Surf. Coat. Technol. 138 (2001) 135–140.
[35] M.M. Bergshoef, G.J. Vancso, Adv. Mater. 11 (1999) 1362–1365.
[36] X.Y. Wang, C. Drew, S.H. Lee, K.J. Senecal, J. Kumar, L.A. Samuelson, Nanoletters 2 (2002) 1273–1275.
[37] C.L. Casper, J.S. Stephens, N.G. Tassi, D.B. Chase, J.F. Rabolt, Macromolecules 37 (2004) 573–578.
[38] D.A. Czaplewski, S.S. Verbridge, J. Kameoka, H.G. Craighead, Nanoletters 4 (2004) 437–439.
[39] R.C. Ropp, J. Electrochem. Soc. 165 (1968) 841.
[40] J. Dexpert-Ghys, R. Mauricot, M.D. Foucher, J. Lumin. 69 (1996) 203–215.
[41] R.P. Rao, D.J. Devine, J. Lumin. 87–89 (2000) 1260–1263.
[42] P. Schuetz, F. Caruso, Chem. Mater. 14 (2002) 4509–4516.
[43] M. Yu, J. Lin, J. Fu, H.J. Zhang, Y.C. Han, J. Mater. Chem. 13 (2003) 1413–1419.
[44] H. Meyssamy, K. Riwotzki, A. Komowski, S. Naused, M. Haase, Adv. Mater. 11 (1999) 840–844.
[45] L.X. Yu, H.W. Song, Z.X. Lu, L.M. Yang, X.G. Kong, J. Phys. Chem. B 108 (2004) 16697–16702.
[46] L.X. Yu, H.W. Song, Z.X. Lu, L.M. Yang, S.Z. Lu, Z.H. Zheng, J. Phys. Chem. B 109 (2005) 11450–11455.
[47] Y.X. Ni, J.M. Hughes, A.N. Mariano, Am. Mineral. 80 (1995) 21–26.
[48] D.F. Mullica, W.O. Milligan, D.A. Grossie, Inorg. Chim. Acta 95 (1984) 231–236.
[49] D.S. Bem, C.P. Gibson, H.C. zur Loye, Chem. Mater. 5 (1993) 397–399.
[50] P. Núnez, S. Trail, H.C. zur Loye, J. Solid State Chem. 130 (1997) 35–41.
[51] A. Boultif, D. Louër, J. Appl. Crystallogr. 37 (2004) 724–731.
[52] A. C. Larson, R.B. von Dreele 1994 GSAS: General Structure Analysis System ANSCE, MS-H805 (Los Alamos, NM: Los Alamos National Laboratory).
[53] A.L. Bail, H. Duroy, J.L. Fourquet, Mater. Res. Bull. 23 (1988) 447–451.
[54] R.V.N. Krishappa, K. Desai, C. Sung, J. Mater. Sci. 38 (2003) 2357–2365.
[55] D. Li, Y.N. Xia, Adv. Mater. 16 (2004) 1151–1170.
[56] Y.F. Zhang, J. Yang, Q. Li, X.Q. Cao, J. Cryst. Growth 308 (2007) 180–184.
[57] J.S. Travis, A.V.R. Horst, Biomaterials 29 (2008) 1989–2006.

[58] K. Riwotzki, H. Meyssamy, H. Schnablegger, A. Kornowski, M. Haase, Angew. Chem., Int. Ed. 40 (2001) 573–576.
[59] V. Buissette, M. Moreau, T. Gacoin, J.P. Boilot, Adv. Funct. Mater. 16 (2006) 351–355.
[60] O. Lehmann, K. Kömpe, M. Haase, J. Am. Chem. Soc. 126 (2004) 14935–14942.
[61] K. Kömpe, H. Borchert, J. Storz, A. Lobo, S. Adam, T. Möller, M. Haase, Angew. Chem. Int. Ed. 42 (2003) 5513–5516.
[62] M. Yu, H. Wang, C.K. Lin, G.Z. Li, J. Lin, Nanotechnology 17 (2006) 3245–3252.
[63] J.X. Wan, Z.H. Wang, X.Y. Chen, L. Mu, Y.T. Qian, J. Cryst. Growth 284 (2005) 538–543.
[64] J. Yang, X.M. Liu, C.X. Li, Z.W. Quan, D.Y. Kong, J. Lin, J. Cryst. Growth 303 (2007) 480–486.
[65] J. Yang, C.X. Li, Z.Y. Cheng, X.M. Zhang, Z.W. Quan, C.M. Zhang, J. Lin, J. Phys. Chem. C 111 (2007) 18148–18154.
[66] C. Feldman, Phys. Rev. 117 (1960) 455.